Computers and Electronics in Agriculture 232 (2025) 110110

Contents lists available at ScienceDirect

Computers and Electronics in Agriculture

journal homepage: www.elsevier.com/locate/compag

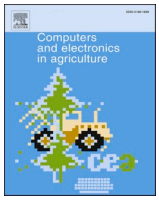

A comparison of proximal and remote optical sensor platforms for N status estimation in winter wheat☆

Francesco Argento [a,*], Quirina Merz [b], Gregor Perich [b], Thomas Anken [c], Achim Walter [b], Frank Liebisch [a]

[a] Water Protection and Substance Flows, Agroscope 8046 Zürich, Switzerland
[b] Crop Science, ETH Zürich, Universitätstrasse 2 8092 Zürich, Switzerland
[c] Digital Production, Agroscope 8356 Ettenhausen, Switzerland

ARTICLE INFO

Keywords:
Optical sensors
Winter wheat
Nitrogen status
Nitrogen fertilization

ABSTRACT

Monitoring crop N status by means of proximal and remote sensing data can help enhancing N use efficiency at various farm scales. This study compares five optical sensor platforms, commonly used in practice and research, based on their usability and accuracy in measuring crop N status at field level. The data were gathered in 2019 in two sites in northeast Switzerland that were cropped with winter wheat (*Triticum aestivum*). The optical sensor platforms employed included a Sentinel-2 satellite, two different unmanned aircraft systems (UAS fixed-wing and quadcopter), a tractor-mounted system, and a handheld field spectrometer. We used a power regression to compare the measured crop N uptake with spectral vegetation indices computed from the different sensors. The reported normalized difference red-edge (NDRE) index values were distributed in a broad range from 0.17 to 0.74, with the Sentinel-2 satellite records in the higher part of the range (0.59–0.74) and those of the handheld spectrometer in the low range (0.17–0.29). The study's key finding was the information collected was significantly different across the five sensing platforms, in terms absolute values from the sensors. However, the correlations between NDRE values from all sensors and the measured N uptake were comparably robust, with $r > 0.8$ a root mean square error ranging from 29 to 37 kg N/ha. Furthermore, the N application maps produced for the satellite and UAS platforms showed that the best compromise between detailed spatial resolution and matching of the working width of the machinery used was achieved by resampling the UAS-based maps at 10 m resolution with the calculation used in this study. We concluded that sensor-based N status assessment across different sensing levels can support the improvement of N use efficiency by allowing a more precise management of in-field variability, with the precondition of having a good calibration for climatic location and variety. However, factors such as the degree of detail needed to capture in-field variability while matching the working width should be evaluated for each specific case.

1. Introduction

Finding solutions to reduce the adverse consequences of imprecise nitrogen (N) fertilizer application at different farm scales is necessary. To better understand and manage N flows in the agro-ecosystem, proximal and remote sensing information from crops can be valuable (Corti et al., 2018; Scharf et al., 2002; Wang et al., 2019; Warner et al., 2009). In fact, the distribution of N available to the plant is often heterogeneous at field-level, as it is influenced by several environmental and management factors (Kindred et al., 2015; Williams et al., 2016). Therefore, using site-specific management strategies based on optical sensors that consider the spatial dynamics on N demand from the crop and N supply from various inputs, such as soil and fertilizer, can lead to improved nutrient use efficiency (Coquil and Bordes, 2005; Cohan et al., 2018; Heege et al., 2008; Mittermayer et al., 2021; Mulla, 2013; Walter et al., 2017). Significant gains in N use efficiency have been shown in a number of field studies that compare sensor-based N management with conventional farming approaches (Aula et al., 2020; Sharma and Bali, 2017). In these studies, the risk of N loss was reduced without lowering yields or affecting quality (grain protein content). Moreover, it was

☆ This article is part of a special issue entitled: 'Precision Nutrient Management' published in Computers and Electronics in Agriculture.

* Corresponding author.
E-mail address: francesco.argento@agroscope.admin.ch (F. Argento).

https://doi.org/10.1016/j.compag.2025.110110
Received 11 October 2024; Received in revised form 7 February 2025; Accepted 7 February 2025
Available online 22 February 2025

shown that with sensor-based approaches for N management, N fertilizers were saved from 4 % up to 46 % (Colaço and Bramley, 2018; Koch et al., 2004) and N surplus in the soil was reduced up to 30–50 % (Diacono et al., 2013).

1.1. Proximal and remote sensing for monitoring vegetation and N-status

With numerous proximal and remote optical sensing platforms, using spectral data to monitor canopy structure and plant growth dynamics has led to better understanding of plant growth and nutrient uptake (Gabriel et al., 2017; Roberts et al., 2012; Samborski et al., 2009). In this study, we refer to optical sensors as sensors or cameras that collect spectral information and to platforms as the carriers of the sensors, which can be, for example, a satellite-platform, an unmanned aircraft system (UAS) or a tractor. At present, many optical sensor platforms operating at various levels of proximity and automation are used for precision agricultural applications on land vehicles (Gnyp et al., 2016; Mezera et al., 2021), as well as on UASs (Bendig et al., 2015; Raj et al., 2020), and satellite platforms (Magney et al., 2017; Perich et al., 2021). Mainly multispectral sensors providing highly-resolved spatial and temporal data are used for precision farming practices to monitor crop development and make crop management decisions (Jin et al., 2017). To calibrate the sensors' data appropriately, however, data on plant parameters—such as dry matter, N concentration, and N uptake—are frequently required (Perich et al., 2021).

Different approaches have been developed for monitoring crop N status, from hyperspectral and multispectral spectroscopy, used to compute spectral vegetation indices (SVI) (Cammarano et al., 2011; Barnes et al., 2000; Li et al., 2014; Zhao et al., 2018) to radiative transfer models (Féret, 2011). It has been demonstrated that the crop's spectral signature shows constant shifts depending on the N status and that the SVIs calculated from the near-infrared (NIR) band provide the most relevant information, as light reflectance has higher values compared to the visible region (Guyot et al., 1988; Raun et al., 2005; Tucker, 1979). In practical applications to crop management, numerous studies have used SVI to estimate specific regions of the electromagnetic spectrum, commonly between the R (620–700 nm) and NIR region (790–840 nm) (Berger et al, 2020; Muñoz-Huerta et al., 2013). Several crops, such as wheat, maize, and sugar beet, exhibit a consistent direct association between this region and their biomass and N status (Bean et al., 2018; Li et al., 2018; Prey and Schmidhalter, 2019). Inside this region of the spectrum, indices such as the normalized vegetation index red-edge index (NDRE) are superior to other indices such as the normalized difference vegetation index (NDVI) because they are less affected by canopy saturation in dense vegetation and provide better sensitivity to variations in chlorophyll content and nitrogen status (Argento et al. 2021; Magney et al., 2017). In most cases, the estimation of the N status via proximal or remote sensing needs to be translated into an N application map to be useful in practical site-specific nutrient management at the field level. The exception is automated systems on the move (on-the-go), in which data are processed online in the field by edge computing. Several approaches and algorithms are used in decision-support systems to create a fertilizer recommendation, but they typically require an expert evaluation. Examples can be found at research (Basso et al., 2016; Liebisch et al., 2014; Samborski et al., 2009) and commercial levels in large areas (Coquil and Bordes, 2005). One additional key aspect of creating an application map is the issue of matching the resolution of the information provided by the different optical sensors to the practical working width in the field so that the information can be used at an optimized level.

Effective N uptake assessment is crucial for optimizing fertilization strategies. The comparison of multiple optical sensor platforms aims to determine their reliability in estimating vegetation indices linked to crop nitrogen status from different sensors and thus farm implementation approaches. It is important for users to know the practical advantages and limitations of each technology, therefore providing a more solid ground for better-informed decisions on investments and use by precision agriculture actors.

1.2. Motivation for the study

Currently available optical sensor platforms for vegetation and N status monitoring provide different information on various temporal and spatial levels. Using these technologies allows us to better determine plant needs and improve the efficiency of N fertilizer use, thereby reducing N surplus risk in crops such as winter wheat. The choice of platform is often dictated by budget restrictions and project-specific objectives and constraints. Relevant knowledge to support this choice is the comparability of the information from different platforms and its effects on certain applications. To address this gap, the present study undertakes a comparative analysis of five distinct optical sensor platforms that are readily accessible on the market and are frequently employed in both practical agricultural applications and research for monitoring N status in winter wheat. The platforms are discussed based on the literature, integrated with a practical example based on data from a field experiment with winter wheat conducted in Switzerland in 2019. The main objective of the study was to quantitatively assess whether the spectral information provided by the five platforms performs similarly for monitoring the N-status of winter wheat. The secondary objective was to show the potential differences for the creation of an N status and application maps from the spectral information for site-specific management from various optical sensor platforms and their application at different spatial resolutions.

2. Methods

2.1. Study location and choice of optical sensor platforms

A case study was used as base for the comparison of the spectral sampling with five distinct optical sensor platforms. The choice of optical sensor in the case study reflects typical market availability as well as availability at the partner institutions participating in the study in the season chosen (Fig. 1a-e). The data for the case study were gathered in 2019 in two sites (F2 & F3, Fig. 1f) in northeast Switzerland where winter wheat (*Triticum aestivum*), cultivar Arnold (Saatzucht Donau, Austria), was planted. The names of the fields were kept as in the original study (Argento et al., 2020, 2022) for consistency with the published material (field F1 is not included in this study).

The five employed optical sensor platforms were selected according to availability at research farm and time of the experiment and to be representative of different, commercially-available sensing levels (Fig. 1, a-e). The satellite platform of choice was Sentinel-2 satellite of the Copernicus Mission from the European Space Agency orbiting at ~ 790 km from Earth (Fig. 1a). The satellite is equipped with a Multispectral Instrument (MSI), a passive sensor with a field of view of 290 km and a temporal resolution (revisit time) of 5 days. The MSI has a spectral resolution of 13 spectral bands distributed across the visible and near-infrared (NIR) spectrum (Fig. 2) and a spatial resolution between 10 and 60 m depending on the band (ESA, 2023). In Fig. 2, for the MSI and multispectral cameras, the bands were used according to the source (ESA) or producer (MicaSense and Parrot). For the Isaria sensor, the range is assigned following Mezera et al. (2021), and for the ASD Spectrometer, the full range is shown, given that the sensor has a hyperspectral range.

The fixed-wing UAS platform is a WingtraOne (Wingtra AG, Zurich, CH; Verling et al., 2017) (Fig. 1b). Flight height was 100 m (Table 1) with a side overlap of 80 %. The UAS was equipped with a 5-band multispectral camera, RedEdge-M (MicaSense, Seattle, USA). The camera measured a blue (B) band at 475 nm (20 nm full-width half max (FWHM), a green (G) band at 560 nm (20 nm FWHM), a red (R) band at 668 nm (20 nm FWHM), a red-edge (RE) band at 717 (10 nm FWHM), and a NIR band at 840 nm (40 nm FWHM) (Fig. 2). For additional

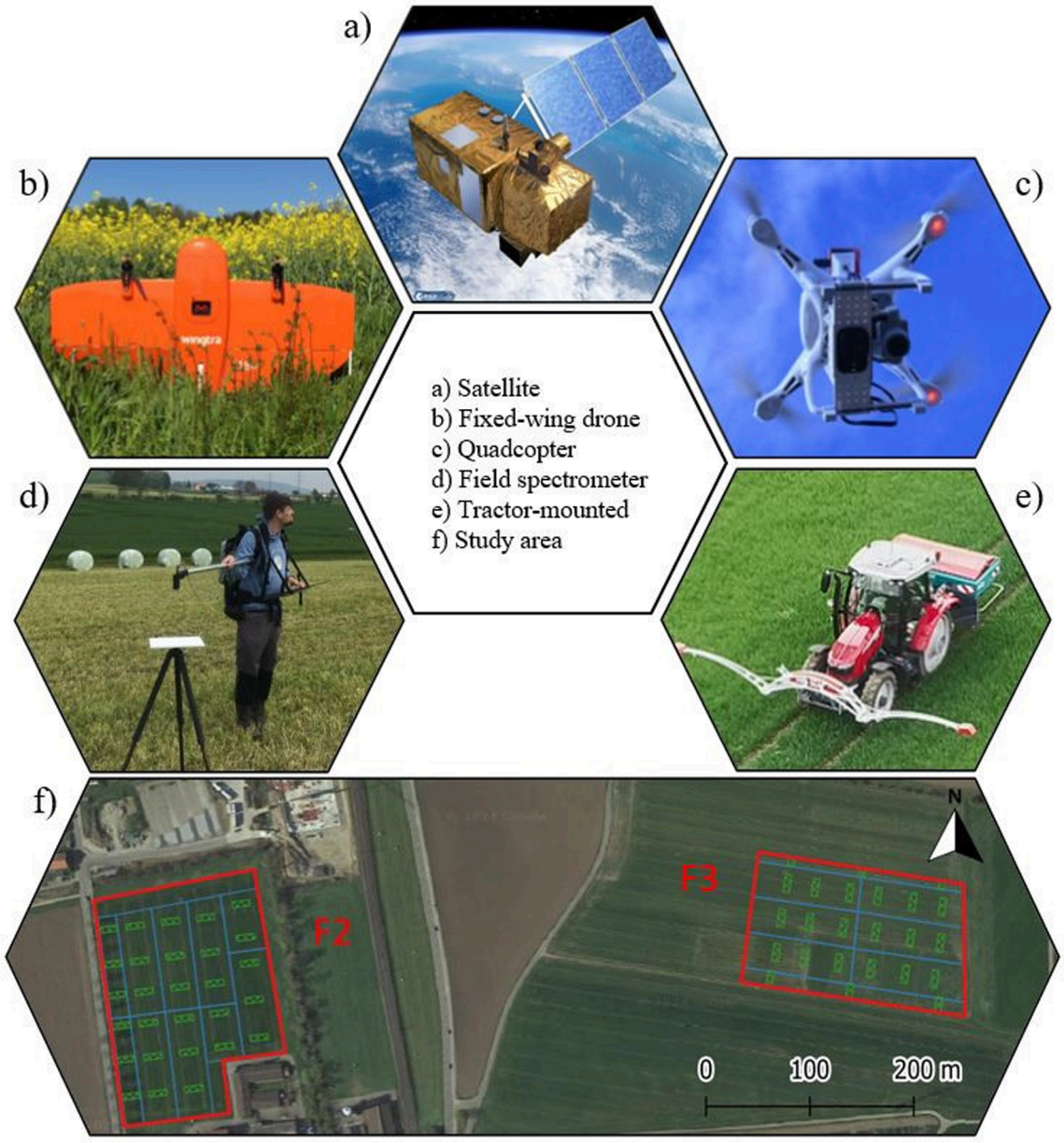

Fig. 1. Optical sensor platforms (a) a Sentinel-2 satellite platform (ESA, 2023), (b) a Wingtra unmanned aircraft system (UAS, fixed-wing), (c) a DJI Phantom UAS (quadcopter), (d) a tractor-mounted system, and (e) an ASD hand-held field spectrometer. Location overview of the case study: f) experimental fields F2 and F3. Source for base orthophoto in (f): Google Maps®.

information refer to Merz (2022). The quadcopter UAS platform was constituted by a Phantom 4 Pro (DJI, Shenzhen, China) equipped with a "Sequoia" multispectral camera (Parrot, Paris, France) (Fig. 1, c). Four bands were used to record the crop's spectrum data (Fig. 2), namely G centered at 550 nm, R centered at 660 nm, RE centered at 735 nm, and NIR centered at 790 nm, with a bandwidth of 10 nm for the RE and of 40 nm for the G, R and NIR channels. The ground sampling distance (GSD) was 8.4 cm pixel^{-1} at 80 m flight altitude (Table 1) and 70 % overlap. For further details refer to Argento et al. (2020).

The tractor-mounted ISARIA proximal crop active sensor system (ISARIA Digital Farming, formerly Fritzmeier, Aying, DE) was used as a tractor-based sensor. The sensor (Fig. 1d) measures at a height of 50–100 cm above the crop with four active LEDs (Table 1) at four spectral wavelengths in the range 660–780 nm (Fig. 2, Mezera et al., 2021). The output was recorded as two indices: the Isaria Biomass Index (IBI), related to biomass and calculated from reflectance in the visible R and NIR radiation and the Isaria Reflectance Measurement Index (IRMI), proposed to be related to N nutritional status based on the reflectance of the R, NIR, and RE spectral bands. The sensor was not connected to the fertilizer spreader in an "on-the-go" system but operated for monitoring purposes only. The field spectrometer ASD FieldSpec4® (ASD Inc., Malvern Panalytical, Malvern, UK) was used as a hand-held sensor (Fig. 1, e). The FieldSpec4 was operated manually at plot level to collect reflectance data from the crop at an approximate height if 100 cm above the ground (Table 1). The spectrometer had a continuous range in the interval 350–2500 nm, which was subsequently resampled to 1-nm bands (Fig. 2).

2.2. Field management and sampling

The two fields F2 and F3 (Fig. 1f) were part of a larger project to test variable rate N application in medium- to small-scale fields (Argento,

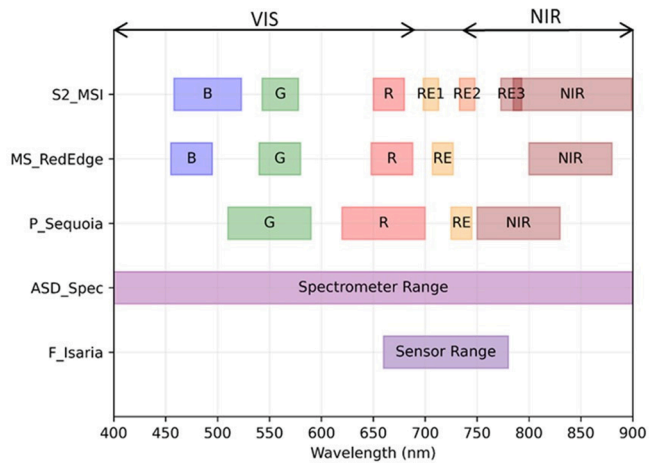

Fig. 2. Visual comparison of the bands of the five optical sensors in the range of visible to near-infrared: Sentinel-2 satellite Multispectral Instrument (MSI; ESA, 2023), MicaSense RedEdge multispectral camera, Parrot Sequoia multispectral camera, tractor-mounted Isaria sensor from Fritzmeier, and ASD field spectrometer.

2021) and were divided into 30 × 90 m plots (30 x 45 m for two plots in field F2) with different N-fertilizer treatments: a variable-rate application with ranges varying from 95 to 149 kg N/ha and a farm standard treatment of 155 kg N/ha of mineral fertilizer (ammonium nitrate 27.5 % N) application and controls with no applied fertilizer. This study focused on the interaction between sensors and plant traits rather than on the fertilizer treatments. Therefore, the treatments are not described in detail; however, there is a detailed description of the experiment for reproducibility in previous studies (Argento et al., 2020, 2022; Argento, 2021; Perich et al., 2021, 2023).

To collect the plant samples, in each field each fertilization plot was divided in two to three subplots of 30 x 30 m and crop data were collected from an undisturbed area of 10 x 30 m inside the subplot. In this area, a metal frame of 0.5 x 0.5 m was randomly placed on the ground and the crop cut at soil level (~1 cm). This process was repeated two times to obtain two frame-cuts of plant material, which were collected in one bag for each of the subplots. This process generated in total 52 bags of plant material, 28 for field F2 and 24 for field F3. The fields were sampled at two different time points during the season. The mid-season sampling took place around 15 April 2019 (± 2 days) corresponding to the second split application of fertilizer (BBCH 31, beginning of stem elongation, according to Meier et al., 2009). The late-season sampling took place around 15 May 2019 (± 2 days) corresponding to the time of the third split fertilizer application (BBCH 37, flag leaf). The plant material was dried at 40 °C for 48 h and grounded into fine material for further analysis of N concentration (N_{conc}). The final dataset was therefore composed of 104 samples of plant dry biomass and N uptake (N_{up} = biomass per area × N_{conc} in crop). Further details about sampling and analysis methods for plants and soil can be found in Argento et al. (2020, 2022).

2.3. Data collection and data processing for sensor comparison

The corresponding spectral data from the different optical sensor platforms were collected around the same date of the two biomass samplings (± 2 days) (15 April 2019 and 15 May 2019), with the workflow shown in the diagram inf Fig. 3. The Sentinel-2 satellite images, for which the scenes were filtered for clouds twice: once on the full S2 tile (100 × 100 km) for cloud cover < 75 % and once on the field level (individual shapefile) for cloud cover < 0 % resulting in the selection of two images (20 April 2019 and 30 May 2019). The spectral data (except for the tractor-mounted sensor) were pre-processed to obtain reflectance data. Data processing pipelines can vary depending on the optical sensor platform used. For satellite data, the service provider performs basic processing, such as georeferencing and terrain correction (ESA, 2023). The Sentinel-2 imagery used in this study was provided with atmospheric correction by ESA (L2A product). The Sentinel-2 images were downloaded in atmospherically corrected L2A format from the 'Creodias' platform. The pre-processing was carried out as described by Perich et al. (2023): (1) for each scene, the 20 m bands were resampled to 10 m using 'cubic' interpolation settings and all bands were written to a 10-band stacked TIFF file (Perich et al., 2023), (2) plot-level reflectance was extracted using the custom-written Python-package 'EOdal' (Graf et al., 2022), and (3) filtered by clouds using the cloud mask provided by ESA.

Image data (single images) from the UAS were stitched together in the software Pix4D Mapper (Pix4D, Lausanne, CH, V4.6.1) for the Sequoia camera and the software Agisoft Metashape (Agisoft, St. Petersburg, RU) for the RedEdge camera with a structure-from-motion approach to create map layers for further analysis. Both output maps for the two UAS platforms were processed by calibrating the raw images using a reflectance target (Airinov and MicaSense). The output maps were spatially corrected by means of ground control points (GCPs). The post-processing pipeline required to extract field-specific data was then similar for the atmospherically corrected L2A Sentinel images and the UAS images. Geospatial analysis and data extraction were carried out for all image data using the QGIS software (QGIS Development Team, 2023, version 3.22.3) and automatized in pipelines with the programming languages R and Python. On-the-go tractor-based sensors do not need external geo-referencing because of the internal link of the machinery with the d-GPS. For the Isaria sensor, we therefore extracted the map for the indices, as provided by the sensor, without additional processing. The spatial point data were recovered from the tractor terminal as

Table 1
Overview of different proximal and remote optical sensing platforms used in the study and their properties. The term platform comprises the carrier of the sensor such as a satellite, an unmanned aircraft system (UAS), a tractor, or an operator. The optical sensor is the physical sensor /camera that is used for collecting spectral information.

Platform	Optical sensor	Type[a]	Distance to crop	GSD	Spectral resolution	Digitization Footprint[b]
Sentinel-2 Satellite	Multispectral Instrument	P	786 km	10–60 m/ px	13 bands 443–2190 nm	0.0007 MB/ ha
Wingtra UAS fixed-wing	MicaSense, RedEdge	P	70–120 *m*	5–10 cm/ px	5 bands 475–840 nm	1000 MB/ ha
DJI P4 UAS quadcopter	Parrot, Sequoia	P	50–100 *m*	5–10 cm/ px	4 bands 550–790 nm	800 MB/ ha
Tractor	Isaria®, Fritzmeier	A	0.5–1 *m*	~cm	Several bands 660–780 nm	0.25 MB/ ha
Hand-held from operator	FieldSpec4®,ASD	P	0.5–1 *m*	~cm	Continuous range 350–2500 nm	125 MB/ ha

[a] Type of sensor: A = active sensor with own light source; P = passive sensor measuring reflection of sun light.
[b] Digitization footprint with raw output information of the sensor as indicator (Marinello et al., 2019).

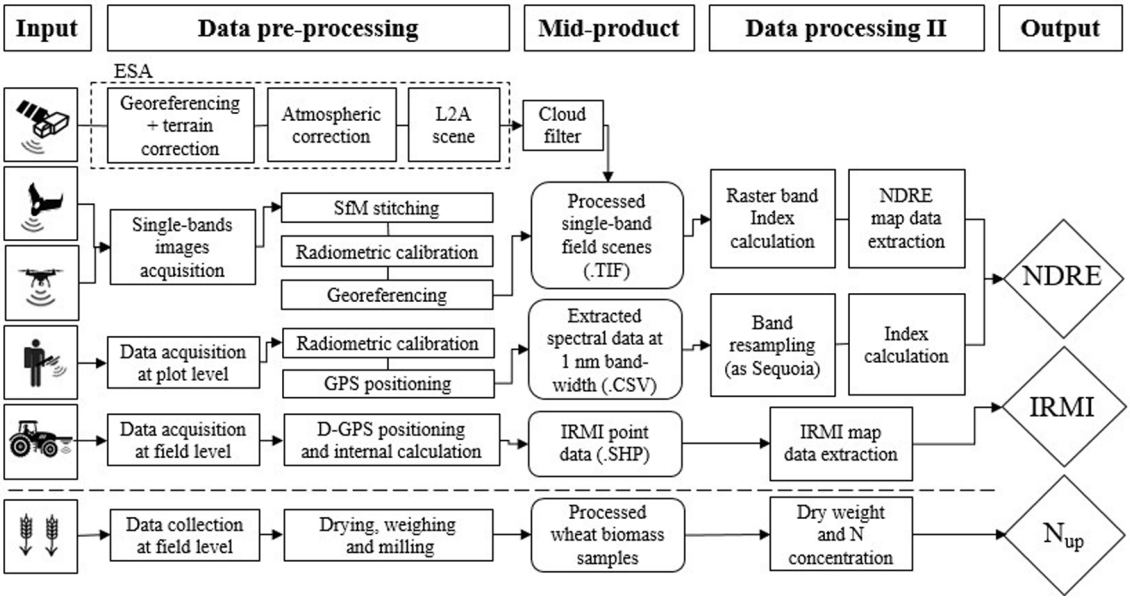

Fig. 3. Diagram of the pre-processing workflow of the spectral information for the five optical sensor platforms to produce the spectral indices NDRE and IRMI, and of the plant data to obtain the N uptake. The workflow was repeated at BBCH31 and BBCH32 for the 52 sampling polygons for a final dataset of 104 data point of N uptake, NDRE and IRMI.

"shapefile"). As reported by Mezera et al. (2021), To minimize the impact of boundary effects, points as far as 20 m from the plot boundaries were removed from the dataset. The ASD was calibrated with a white reflectance panel before each measurement. The output values were recorded in a CSV file containing reflectance for each band and sampling plot, and the GNNS position (coordinates) of each measurement was later assigned to the corresponding sampling plot (see Fig. 1f, green polygons). The four spectral bands corresponding to those of Parrot Sequoia (authors' choice) i.e., RE centered at 735 nm, and NIR centered at 790 nm, with a bandwidth of 10 nm for the RE and of 40 nm NIR channels were extracted for further analysis.

The data were organized in polygons (green polygons with cross lines fill in Fig. 1, f) i.e., the measured N_{up} value was assigned to each polygon and the spectral information (NDRE or IRMI) was extracted for all devices in that same polygon. A regression was done by using the data of measured N_{up} vs the corresponding NDRE value. For the statistical analysis, the base R function nls in R (version 3.6.3; R Core Team, 2024) was used for the power regression between N_{up} and the normalized difference red-edge index, calculated with the following formula according to Barnes et al. (2000): NDRE = [NIR – RE] / [NIR + RE], and the IRMI index (Mezera et al., 2021).

For all spectral data, polygons corresponding to the sampling area of the corresponding plot were used to extract the spectral information so that it was directly comparable with the corresponding crop sample and N_{up}. For Sentinel-2, the band 8 and resampled band 5 were used for calculating the NDRE. For the multispectral cameras the corresponding NIR and RE bands were used as reported in section 2.1 and for the ASD the resampled NIR and RE were used. For the correlation, the root mean square error (RMSE, kg N/ha) and mean absolute error (MAE, kg N/ha) were calculated. The predicted N_{up} was compared to plant measured N_{up} by means of Passing-Bablok regression (mcr package in R; Manuilova and Schuetzenmeister, 2021). Additionally, also the Lin's concordance correlation (DescTools package in R; Signorell, 2021) was computed. The Pearson's correlation coefficient (r) and Lin's concordance correlation coefficient (CCC) are reported. The statistics for the range of the values within the maps: min, max, median, and coefficient of variation (CV) were extracted from the maps and calculated with R (version 3.6.3; R Core Team, 2024).

An ANOVA test was carried out to explore the differences between the ranges of the sensor values. ANOVA was chosen because the data involve multiple groups (different devices) with NDRE measurements, and ANOVA efficiently compares the means across more than two groups. It reduces the risk of Type I errors compared to using multiple t-tests and provides a robust framework for testing overall group differences. A Tukey's HSD post-hoc test was then used to identify specific pairwise differences.

2.4. Data processing and analysis of the simulated N application maps

The calculated output NDRE maps from the section above were used to calculate an example of output N application maps for the two UAS platforms and for the Sentinel-2 data. The strategy used was to redistribute spatially more N fertilizer to pixels with lower NDRE values and vice versa. The calculation was done at pixel level with the formula $N_{fert} = N_{ST} - N$ correction from Argento et al. (2021), in which the reference value (N_{ST}) was the standard application decided by the farm manager and the N correction was calculated by multiplying a correction factor (reflectance at single pixel – value of the field mean reflectance normalized by the field mean reflectance) for N_{ST} to obtain the he relative conversion of reflectance into kg N/ha px^{-1}. This conversion was done for two scenes representing the time of two different split fertilizer applications: the second split fertilizer application at growth stage BBCH 31, based on a reference value of 60 kg N/ha, and the third split fertilizer application at BBCH 37, based on a reference value of 25 kg N/ha.

The statistics for the ranges of the values (minimum, maximum, median, and CV) were extracted from the maps and calculated with the software R version 3.6.3 (R Core Team, 2024). The maps for the same three optical sensor platforms were then resampled by using the 'nearest neighbor' function in QGIS (V 3.22.3) at three different spatial resolutions of 1.5, 10, and 30 m to match the potential tractor's working width at one growth stage (BBCH 31), corresponding to the second split fertilizer application, based on a reference value of 60 kg N/ha. For the resampling, the bilinear resampling function of the Rasterio package (Gillies et al., 2013) in the programming language Python version 3.11.5 was employed. All maps were also cropped with a 10-m buffer from the field borders to exclude any influence of the field margins.

3. Results

3.1. Comparison of spectral information

A comparison of the output captured with the five different optical sensor platforms is reported in this section. As an example, different output maps of the same scene in mid-May 2019 for field F2 (winter wheat) are illustrated in Fig. 4. Two main clusters can be identified in the maps: spatially continuous pixel-based maps (Fig. 4a–c) deriving from the two UAS platforms and the Sentinel-2 scene and a point-based map resulting from the tractor-mounted sensor and the field spectrometer (Fig. 4d, e).

The NDRE values were distributed in a broad range, from 0.17 to 0.74 (Fig. 4 and Table 2). Notably, the distribution of the values was significantly different across the optical sensors, as shown in Fig. 4. The Sentinel map (GSD 10 m) reported a more homogenous pixel color distribution corresponding to higher NDRE values, with a median of 0.74 and a CV of 6.59 %. The Mica Sense map (GSD 10 cm) reported lower values, with a median of 0.56 and a CV of 4.32 %. By contrast, the Sequoia map (GSD 5.4 cm) had a median of 0.43 and a CV of 7.69 %. Lastly, the NDRE values calculated in the point-based ASD map had a median of 0.29 and a CV of 11.85 %. The IRMI absolute values were not comparable to NDRE values; however, the CV of 4.86 % was in the lower range of the other instruments.

An ANOVA test showed that the differences between the means of the value ranges due to the effect of the sensor were significant ($p < 0.001$). The strong effect of sensor type on NDRE values was confirmed by calculating effect size ($\eta^2 = 0.95$), indicating substantial differences between optical sensors. The post-hoc Tukey's HSD test further showed that each device was significantly different from the others (letters added in Table 2 to the mean). The results of the HSD test indicate that all pairwise comparisons between the devices and their respective NDRE measurements are statistically significant. Specifically, the confidence intervals for the comparisons are as follows: for ASD vs. Sequoia, the interval ranges from 0.173 to 0.222 ($p = 1.15e-14$); for ASD vs. MicaSense, the interval ranges from 0.281 to 0.329 ($p = 1.15e-14$); for ASD_NDRE vs. Sent2_NDRE, the interval ranges from 0.431 to 0.479 ($p = 1.15e-14$); for Sequoia vs. MicaSense, the interval ranges from 0.0828 to 0.131 ($p = 2.51e-14$); for Sequoia vs. Sentinel-2, the interval ranges from 0.233 to 0.282 ($p = 1.15e-14$); and for MicaSense vs. Sentinel-2, the interval ranges from 0.126 to 0.175 ($p = 1.15e-14$). None of the confidence intervals include zero, suggesting significant differences between all pairs.

Table 2
Range and coefficient of variation among the pixel and point values of the NDRE index maps for the different optical sensors for the field F2 at BBCH37 as reported in Fig. 4. The minimum, maximum, mean (with significance levels; $p < 0.001$), and median are reported as NDRE values. The coefficient of variation (CV) is shown as a percentage.

	NDRE				IRMI
	ASD	Sequoia	RedEdge	Sentinel-2	Isaria
Min	0.17	0.38	0.49	0.59	20.53
Max	0.29	0.50	0.58	0.74	25.63
Mean	0.24[d]	0.44[c]	0.55[b]	0.70[a]	24.06[n.a.]
Median	0.25	0.43	0.56	0.72	24.37
CV (%)	11.85	7.96	4.32	6.59	4.86

Despite the significant difference observed in range in the examples above, the regression performed between the NDRE index and the IRMI with the corresponding ground-truth values for N uptake (Nup, kg N/ha) from the two sampling campaigns at BBCH 31 and 37, showed comparable results and patterns (Fig. 5). The Sentinel-2 NDRE values were in

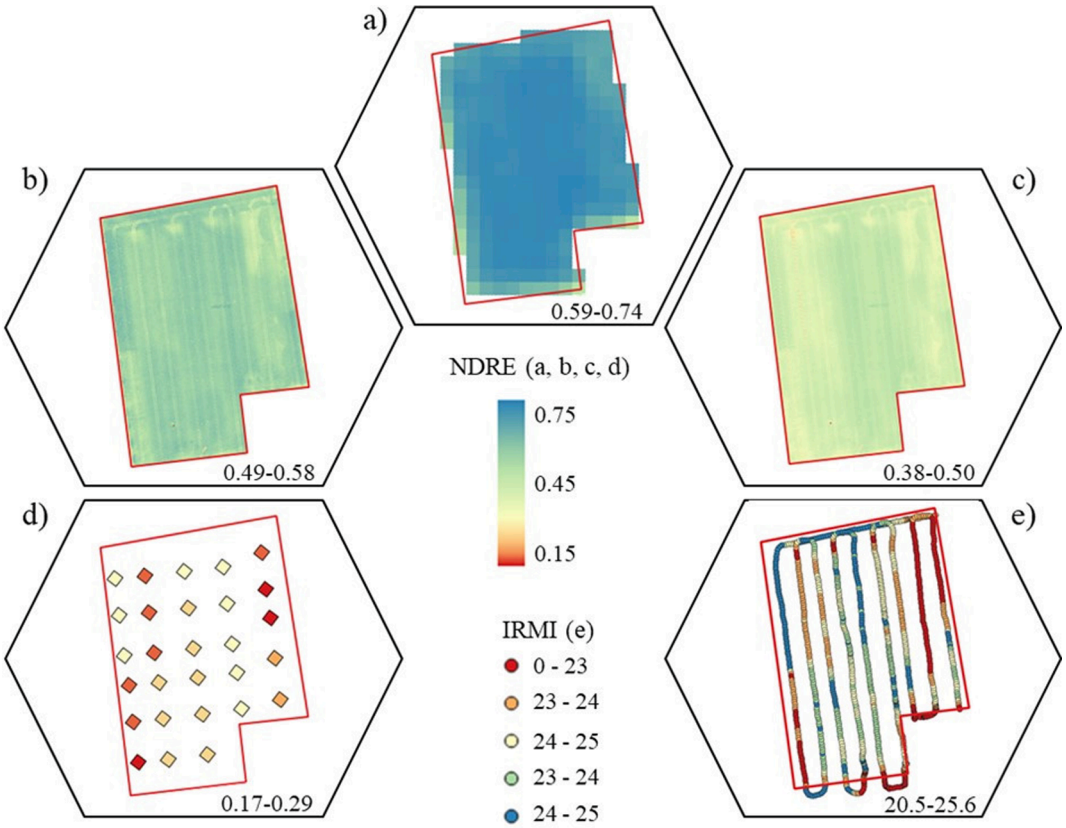

Fig. 4. Normalized difference red-edge (NDRE) index and Isaria Reflectance Measurement Index (IRMI) maps of field F2 from the sampling at BBCH 37 (15 May 2019) for the different optical sensor platforms: (a) Sentinel-2, (b) MicaSense RedEdge, (c) Parrot Sequoia, (d) ASD, and (e) Isaria Fritzmeier (IRMI). The legends for NDRE and IRMI are reported with the individual ranges of each map.

the range 0.55–0.8. The Power and Passing-Bablok regressions based on all Sentinel-2 data were computed on a subset of the original dataset (n = 93) to exclude the points that were biased by "border effects," that is, those whose pixel values were confounded by proximity to the field borders. The points removed from the regression are shown as black dots in Fig. 5a and 5b, while the points used are displayed in orange and green (BBCH 31 and 37, respectively), as in the other plots. The Lin's concordance correlation coefficient (CCC) and Pearson's correlation coefficient (r) for the subset regression between the measured N_{up} and predicted N_{up} were 0.869 and 0.871, respectively.

The NDRE values for the UAS-mounted cameras ranged between 0.35 and 0.6 for the MicaSense RedEdge (Fig. 5c) and 0.2 and 0.5 for the Parrot Sequoia (Fig. 5e). The regression for the RedEdge reported the highest coefficients among all optical sensors, with CCC = 0.875 and r = 0.880 (Fig. 5d), respectively, while it reported CCC = 0.797 and r = 0.817 for the Sequoia (Fig. 5f). The NDRE values for the ASD spectrometer were in the range 0.10–0.30 and the regression resulted in CCC of 0.833 and r of 0.845 (Fig. 5g, h). Finally, for the Isaria sensor, the regression based on the predicted N_{up} from IRMI reported CCC = 0.799 and r = 0.815 (Fig. 5i, j).

The evaluation of the power regression models reported in Table 3 for the two fields F2 and F3 showed different degrees of sensitivity to N_{up} (Fig. 5a, c, e, g, i), depending on the growth stage. The N_{up} values ranged between 30 and 300 kg N/ha. The sensitivity to N_{up} appeared generally higher for the sampling at BBCH 31, with both the root mean square error (RMSE, 10—16, kg N/ha) and the mean absolute error (MAE, 7—12) of the different optical sensors being lower compared to the RMSE (29—41, kg N/ha) and MAE (21—36, kg N/ha) at BBCH 37, as well as to the RMSE (29—37, kg N/ha) and MAE (22–28, kg N/ha) of the full model BBCH 31 + 37. The Sentinel-2 model with excluded values (n = 93) and the MicaSense model reported the lowest RMSE and MAE values for the full model among all optical sensors.

3.2. Calculation of N application maps

In this section, we report an example of parametrization and the creation of an application map from the pre-processed NDRE index maps for three selected platforms (Fig. 6). Handheld sensors are less frequently used for variable rate fertilizer applications, and tractor-mounted sensors are usually integrated in on-the-go systems that need no processing. Therefore, the focus of this section is on the aerial platforms, that is, on the UASs and satellite images. There were differences in patterns between the two scenes, which were taken one month apart, as well as between maps from the different optical sensors for the same scene. The two UASs with high spatial resolution showed similar patterns and values compared to the satellite-based N map, which appeared to be more homogenous in both scenes. This is confirmed by the ranges of the pixel values reported in Table 4. For the Sentinel-2, the CV was the lowest, at 3 % for both vegetation stages, with the values ranging from 56–66 kg N/ha and a median of 60 at BBCH 31 to 24–27 kg N/ha with a median of 25 at BBCH 37.

For the two UAS-mounted optical sensors, the CV was higher at BBCH 31, with 10 % and 14 % for MicaSense and Sequoia, respectively. At BBCH 37, the CV was lower but still higher than the Sentinel-2, with 8 % and 9 % for MicaSense and Sequoia, respectively. The median values of 60 kg N/ha at BBCH 31 and 25 kg N/ha at BBCH 37 were the same for both UAS-mounted optical sensors and also matched the median of the Sentinel-2 sensor.

The range for MicaSense was between 35 and 122 kg N/ha at BBCH 31 and between 17 and 47 kg N/ha at BBCH 37. For Sequoia, the ranges were 20–123 kg N/ha at BBCH 31 and 18–43 kg N/ha at BBCH 37. The extreme values at the margins of the range were likely outliers, and according to the pixel distribution, most values were between 40 and 80 kg N/ha, indicating that the probable range of applications was lower than that observed in the maps.

The resampled N application maps at three possible resolutions (1.5, 10, and 30 m) to match the potential tractor's working width for the three optical sensor platforms at one growth stage (BBCH 31, Fig. 7) showed how the application range can vary significantly depending on the chosen device and the precision of the fertilizer spreader used. At a resampled pixel size of 30 m/px, the overall number of pixels and the relative information in terms of spatial variability were reduced (Fig. 7a–c). Additionally, the algorithm used discarded/kept different pixels for the Sentinel-2 map. At a 10 m/px resolution, which would be the original resolution of the satellite images, the main pattern of within-field variability was still observed in the UAS-based maps (Fig. 7d–f). At 1.5 m, the two UAS-based maps offered a higher level of detail (Fig. 7g–i), but the variance of the satellite maps did not increase.

4. Discussion

This study aimed to evaluate the performance of five commonly used optical sensor platforms in assessing nitrogen status in winter wheat, addressing the practical implications for precision agriculture. Given the varying spatial and temporal resolutions of these technologies, understanding their comparability is essential for optimizing nitrogen management and minimizing surplus risks. By integrating insights from the literature with field experiment data, we assessed the extent to which different platforms provide consistent spectral information for N monitoring in wheat and key differences in their suitability for generating N status maps and guiding site-specific fertilization, emphasizing the importance of selecting the appropriate platform based on specific technical and agronomic aspects.

4.1. N status detection with different optical sensor platforms

The results presented show a significant shift in normalized difference red edge (NDRE) index absolute values (ranges, means and median) between the different optical sensor platforms (excluding the tractor-mounted sensor, having a different range of values), clearly indicating that the information captured differs significantly. This is mainly due to the differences in sensor properties, such as bandwidth and center: the NDRE of Sentinel-2 and MicaSense is calculated with similar bands while the NDRE for the ASD was computed by using the same bandwidth of the Parrot Sequoia. The radiometric resolution may explain the differences between the two groups but inside the same group the Sequoia is significantly different from the ASD and the MicaSense from Sentinel-2. An explanation for these differences could be that the sensors undergo different optical calibration procedures (reflectance panels or atmospheric correction) further influencing the absolute values but not the relative difference between pixels, therefore the range distributions correlate well with each other and with winter wheat N uptake measured analytically, as shown in previous studies (Li et al., 2018; Singh et al., 2015; Zhao et al., 2018). The interpretation of these results suggests that the information provided by the sensors, although differing at absolute values, can be calibrated with analytically measured crop N uptake data to provide similar and meaningful indications of the N status of the crop. Eventually, the differences between the absolute values of the sensors could be mitigated with a cross-calibration that corrects for variations in spectral information (Wang et al., 2024). However, it would require a comprehensive data set containing crop N status standards, as presented in this study, but ideally also optical standards, such as panels with different gray intensities.

4.1.1. Effect of sensor type on data ranges

An examination of the maps generated for field F2 (winter wheat) in mid-May 2019 exemplifies distinct map-type clusters, with unmanned aerial system (UAS) platforms and Sentinel-2 producing spatially continuous pixel-based maps, while the tractor-mounted sensor and field spectrometer generated point-based maps. Notably, the range of NDRE values varies significantly between the different optical sensors, with Sentinel-2 exhibiting a more homogeneous distribution compared

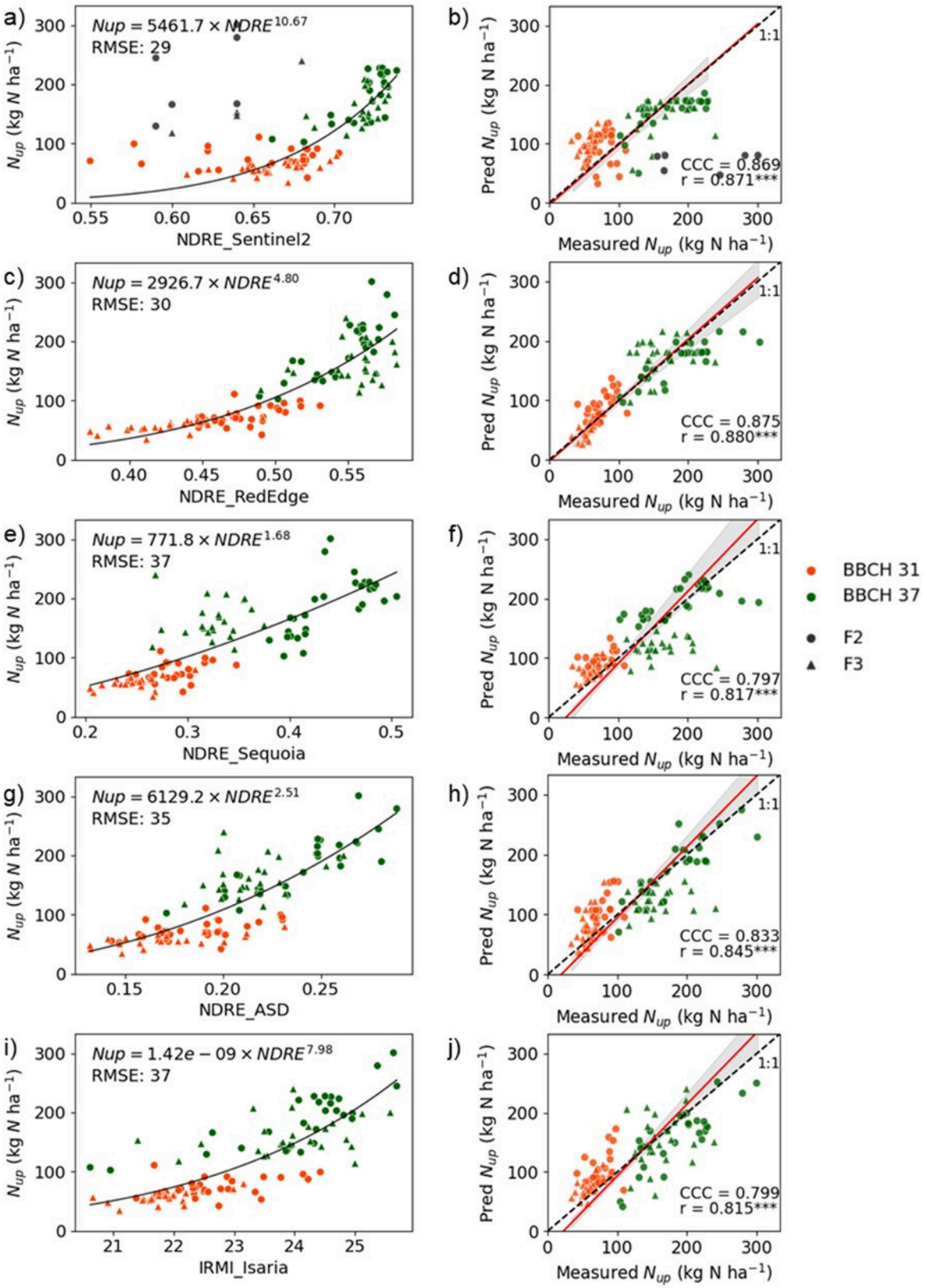

Fig. 5. Power regression between measured N uptake (N_{up}, kg N/ha) and the indices NDRE and IRMI (n = 104) for the two fields F2 and F3 (circles and triangles) and two growth stages BBCH 31 and 37 (orange and green) for the five optical sensors with the corresponding Passing-Bablok regression between the measured N_{up} (kg N/ha) and the predicted N_{up} (kg N/ha).

Table 3
Sensitivity of NDRE and IRMI to the measured plant trait (N uptake) at mid- (BBCH 31, mid-April) and late-season (BBCH 37, mid-May), as well as for the two combined (BBCH 31 + 37), extracted from the different optical sensors. The root mean square error (RMSE, kg N/ha) and mean absolute error (MAE, kg N/ha) of the power regression model for the different optical sensors are reported. Lower error values indicate higher sensitivity.

	BBCH 31		BBCH 37		BBCH 31 + 37	
	RMSE	MAE	RMSE	MAE	RMSE	MAE
	NDRE					
ASD spectrometer	12	9	29	21	35	25
Parrot Sequoia	13	9	38	29	37	27
MicaSense RedEdge	10	7	37	29	30	22
Sentinel-2	16	12	43	36	29	23
			IRMI			
Fritzmeier Isaria	12	8	34	27	37	28

to others. An ANOVA test was carried out to explore the differences between the ranges of the sensor values. ANOVA was chosen because the data involve multiple groups (different devices) with NDRE measurements, and ANOVA efficiently compares the means across more than two groups. It reduces the risk of Type I errors compared to using multiple t-tests and provides a robust framework for testing overall group differences. A Tukey's HSD post-hoc test was then used to identify specific pairwise differences. This approach ensures statistical rigor when analysing NDRE variability.

These results have important implications for the study. The variability observed across platforms suggests that device choice could influence the accuracy and reliability of NDRE measurements. Such variability may impact how NDRE is interpreted in field studies, particularly if the measurements are used for decision-making in nutrient management or crop monitoring. Therefore, the findings emphasize the need to carefully consider the platform used for NDRE measurements in future studies, as different devices may yield different results under the same conditions. Moreover, the statistical significance of these differences suggests that further research is warranted to investigate the causes of this variability—whether it stems from technical differences in sensor calibration, environmental factors, or other variables. Understanding these sources of variability could help standardize NDRE measurements across platforms, leading to more consistent and reliable data for agricultural applications.

Table 4
Range and coefficient of variation among the pixel and point values of the N-status maps for the three optical sensors. The minimum, maximum, and median are reported as kg N/ha. The coefficient of variation (CV) is shown as a percentage.

		N application (kg N/ha)		
		Sentinel-2	**MicaSense**	**Sequoia**
BBCH 31	**Min**	56	35	20
	Max	65	122	123
	Med	60	60	60
	CV (%)	3	10	14
BBCH 37	**Min**	24	17	18
	Max	27	47	43
	Med	25	25	25
	CV (%)	3	8	9

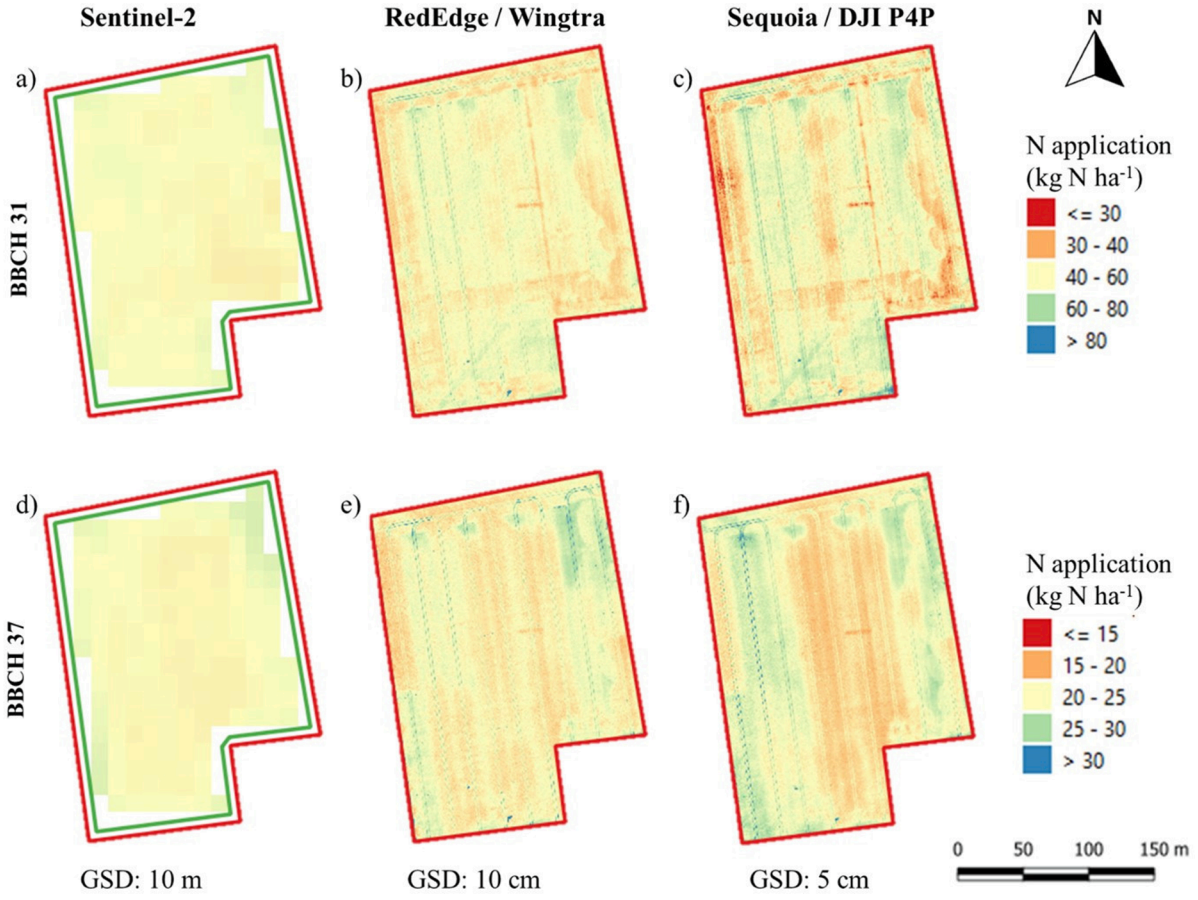

Fig. 6. Theoretical N application map (kg N/ha) based on NDRE for three optical sensor platforms. The two rows report two different split applications: (a–c) at BBCH 31 (ref. value 60 kg N/ha) and (d–f) at BBCH 37 (ref. value 25 kg N/ha). The green lines in (c) and (f) represent a 10-m buffer from the field borders (red).

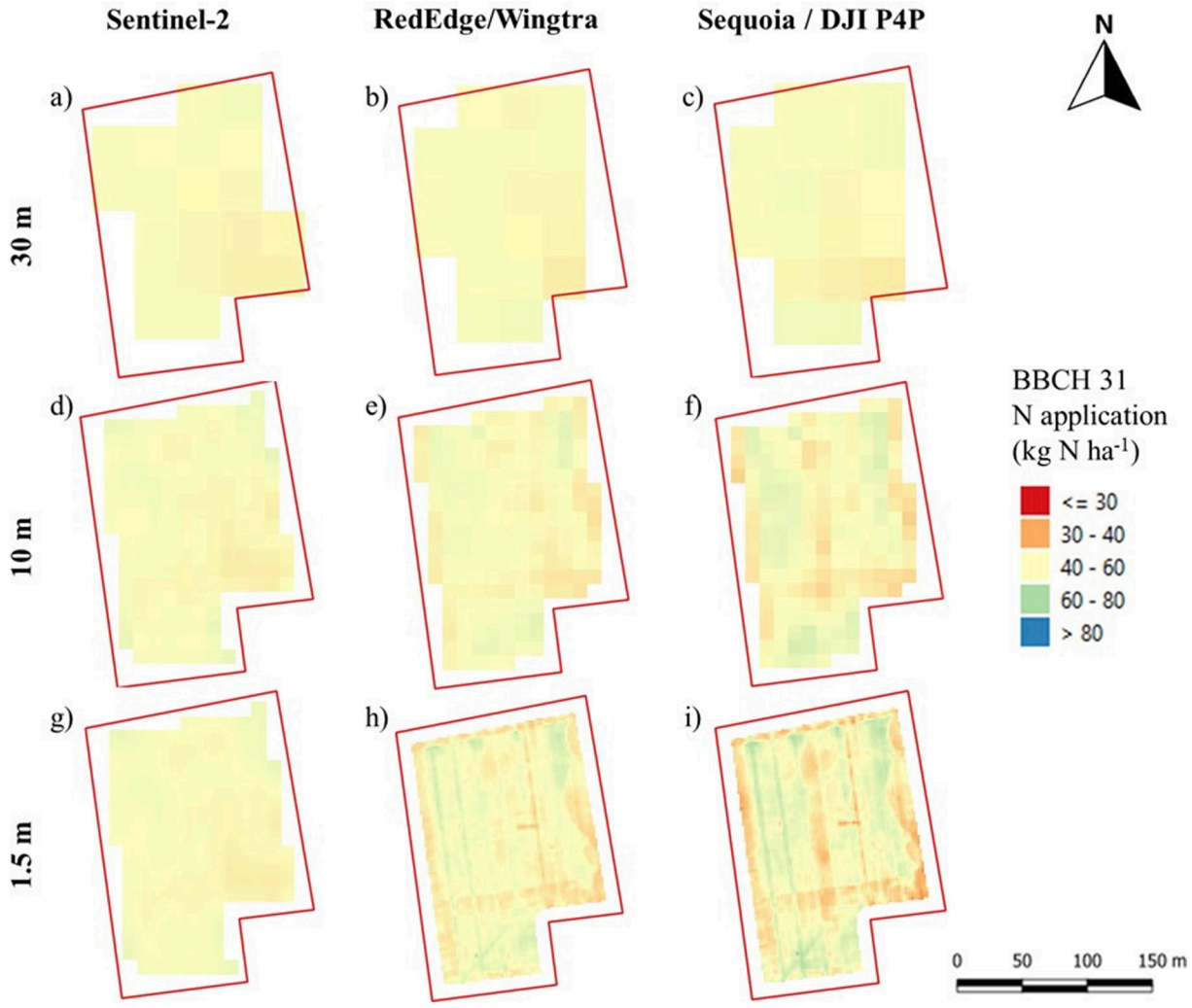

Fig. 7. N application map (kg N/ha) resampled at three spatial resolutions: (a–c) 30 m, (d–f) 10 m, and (g–i) 1.5 m to match the potential tractor's working width for the three optical sensor platforms. Values for one split fertilizer application at BBCH 31 (ref. value 60 kg N/ha). All maps were cropped with a 10-m buffer.

4.1.2. *Choice of spectral vegetation index*

The choice of this spectral vegetation index (SVI) was facilitated by the fact that it has been used in several studies that investigated variable rate N fertilization and remote N uptake estimation due to the use of RE and NIR bands (Barnes et al., 2000; Diacono et al., 2013; Jiang et al., 2021; Prey and Schmidhalter, 2019). In the base study associated with the case study (Argento, 2021; Argento et al., 2022), several SVIs were tested against different plant traits, such as N uptake, N nutrition index, N concentration, and dry biomass. The NDRE had the best relationship with the N uptake of winter wheat. NDRE and IRMI appear superior to the normalized difference vegetation index (NDVI) for in-season nitrogen fertilization decisions because they are less affected by optical saturation in dense vegetation and provide better sensitivity to variations in chlorophyll content and nitrogen status. The saturation effect observed with NDVI (Clay et al., 2012), was not predominant for NDRE in this study, as previously shown (Magney et al., 2017). The IRMI was the SVI provided by the tractor-based sensor provider, suggested to be related to the N status (Mezera et al., 2021). This was confirmed by our study.

4.1.3. *Correlation between NDRE and N uptake*

The analysis of the NDRE values versus crop N uptake revealed differences in value ranges but generally good correlations across optical sensors. The regression analyses highlighted strong correlations between NDRE values and N uptake, particularly evident with the RedEdge and corrected Sentinel-2 full models, which demonstrated the highest correlation coefficients and lowest errors. These two sensors have a similar bands distribution compared to the Parrot Sequoia and the ASD (for which the indices were calculated following the band's structure of Sequoia). Moreover, the study addresses challenges such as border effects. This issue can occur especially for sensors with large spatial resolution, for which the pixels located at the borders may contain information from outside the field borders and therefore be a source of error. This was resolved by excluding pixels that were partly outside the field borders with a subset regression for Sentinel-2 data (Perich et al., 2021). Overall, while each sensor platform offers unique advantages and limitations, its ability to correlate NDRE values with N uptake underscores its utility in precision agriculture applications.

4.2. *Creation of an application map from different sources*

In this section, we discuss the different application maps created utilizing pre-processed NDRE index maps from three selected platforms. Given that handheld sensors are less commonly employed for variable rate fertilizer application and tractor-mounted sensors are typically integrated into on-the-go systems requiring minimal processing, our focus here lies on UASs and satellite imagery. The visual examination of these maps revealed differences in patterns not only between scenes taken one month apart but also among maps from different sensors capturing the same scene. Notably, UASs with high spatial resolutions exhibited (in

much higher detail) similar general field patterns compared to the more homogenous satellite-based N maps in both scenes. These observations show the importance of considering both temporal and spatial variations when implementing precision agriculture strategies and highlight the complementary strengths of UAS and satellite-based approaches in N fertilizer application mapping. In this case study, the satellite-based maps appeared to provide a lower range of fertilizer applications, which may in turn reduce their usefulness for site-specific management. This may be a problem for small-scale fields, but it is very much dependent on inherent within-field variability and should not be generalized based on this study.

4.2.1. Resampling of the N application maps

The resampling of the N application maps at three possible resolutions (1.5, 10, and 30 m) to match potential or common machinery working width for the three optical sensor platforms at one growth stage showed that the application range can vary significantly depending on the chosen device and the precision of the map or used machinery, such as fertilizer spreader used. At a coarser resampled resolution of 30 m, the overall number of pixels and the relative information in terms of spatial variability were reduced. Additionally, the function 'nearest neighbor' used for the resampling had a different output in terms of pixel distribution inside the field borders for the Sentinel-2 map compared to the UAS maps. At 10 m resolution, which would be the original resolution of the satellite images, the main pattern of within-field variability could still be observed even in the UAS-based maps; this seems to be an ideal resolution to match most typically used fertilizer spreaders with a range from 12-30 m working width. At 1.5 m, the two UAS-based maps offered a higher level of detail compared to the satellite map. However, this type of precision can be matched in field management only by a pneumatic spreader with variable section control. Especially for coarser resolution, it is relevant to state that the fixed orientation of the pixels in the maps (N-S) does not match the direction of driving and management in the field. This results in a loss of information and imprecise representation of the fertilizer application zones in the field.

The differences observed in Fig. 6 between UAS-based images and satellite-derived maps highlight the impact of spatial resolution on site-specific nitrogen application. Higher-resolution UAS data (1.5 m) captures finer within-field variability, enabling more precise fertilizer application, while coarser resolutions (10 m and 30 m) may smooth out spatial heterogeneity, potentially leading to suboptimal management decisions. However, the practical relevance of these differences depends on both the working width of the application machinery and the initial assessment of within-field variability. Since identifying variability is the first step in site-specific management, the choice of sensor plays a crucial role in shaping the fertilization strategy. High-resolution sensors may be beneficial for fields with strong spatial heterogeneity, whereas lower-resolution data might be sufficient for more uniform fields, aligning data collection efforts with practical management needs.

4.2.2. Reference values for N application

Finally, it is critical to establish a reference value for spatial N application adjustment. The amount was provided manually in the case study, as the approach was built as a decision-support system. Real-time N sensing coupled with machine learning approaches, such as reinforced learning, could improve estimating this process, which is presently based on best fertilization practices (Jordan-Meille et al., 2023; Sinaj and Richner, 2017), local farming and technical experience. We used the NDRE maps to calculate N application maps for both the UAS platform system and Sentinel-2 data. Following the methodology outlined by Argento et al. (2021), which involves the spatial redistribution of N fertilizer based on NDRE values, we generated maps representing the second and third split fertilizer applications at BBCH 31 and 37, respectively. The reference values, determined by the farm manager, served as standards for converting reflectance into kg N/ha px^{-1}. Spatial variations in crop growth are addressed as a reference to the field mean and therefore also reflects seasonal changes in the vegetation. Because the design contained border, or so-called cut-off values, plots with additional fertilizer and plots without any fertilizer, the mean value of the field's spectral vegetation index was employed in this work. It may not always be the most effective option, though, as this mean value should reflect the ideal crop N status.

The calculation of the N application rate with different algorithms may lead to different results: according to current research, the 95th percentile (Stamatiadis et al., 2018), the median, or the most frequent pixel value may serve as indicators of reference values (Samborski et al., 2009). Other widely used sensing algorithms typically use reference sensor values of a controlled area in which the N status of the crop is estimated to be optimal in conjunction with the sensor values of a target area (Franzen et al., 2016; Padilla et al., 2018; Yao et al., 2015). These algorithms usually make use of a sufficiency index (Holland and Schepers, 2010) or response index of the crop (Raun et al., 2005). These algorithms such as machine learning-based models or those incorporating more detailed environmental variables could offer advantages in capturing crop growth variability more effectively. While the approach used in this study provides a consistent framework for N mapping, it may be limited in its ability to account for complex, dynamic factors such as changes in crop development, soil heterogeneity, and weather conditions over time. Other methods may therefore provide more potential for improving the accuracy and adaptability of N application maps, particularly in variable field conditions.

4.3. Advantages, limitations and error sources of sensor approaches

Different sensor platforms have varying properties, such as distance to the crop and spectral resolution, which can significantly influence the resulting information. Therefore, the use of handheld, tractor- mounted, UAS, and satellite-carried sensors offers distinct advantages and limitations (Muñoz-Huerta et al., 2013; Tremblay et al., 2011). This study addresses the gap in research by comparing different platforms and sensors for N fertilization decision support, offering a comprehensive analysis of their effectiveness in correlating nitrogen uptake with spectral indices. While previous research has focused on individual sensors, this study's comparison allows for a more robust understanding of how each platform captures the relationship between spectral data and nitrogen dynamics. By evaluating the sensors' ability to accurately estimate nitrogen uptake, we provide valuable insights that can guide the selection of the most suitable sensor for N fertilization decisions. Knowing that these sensors can deliver comparable quality of information, empower users to make informed decisions based on practical and financial factors when considering investments and integrating this technology into their farm operations.

4.3.1. Technical strengths and weaknesses of sensor-based nutrient monitoring

Handheld sensors such as field spectrometers or leaf clip sensors provide valuable data for fertilizer management, but their low spatial resolution may limit decision-making for field management and fertilizer application (Chunjiang et al., 2007; Perich et al., 2021). In terms of cost-effectiveness, they are therefore rather low compared to the other (medium to high costs, low resolution and time-intensive). Tractor-mounted sensors offer on-the-go information and automated data processing, making them efficient for variable rate applications (Adamchuk et al., 2004). However, only in certain cases are the calibration and calculation processes transparent (Isaac and Na, 2016). Moreover, in terms of cost-effectiveness they are the simplest to use as no data processing is required but excessive costs may influence their adoption depending also on the farm size (Lowenberg-DeBoer and Erickson, 2019).

Low-altitude remote sensing using UASs allows for high-resolution imagery with high spatial, spectral, and temporal monitoring capabilities. It provides the opportunity to create maps shortly before fertilizer

application (below-clouds) but requires processing knowledge and effort. The cost-effectiveness of commercial UASs and cameras for agricultural applications compared to scientific-grade equipment makes them a potential option, even for small-scale farming. These platforms provide a clear advantage in spatial resolution, allowing for high-precision data collection across large fields. By integrating UAV-based optical sensors, farmers can achieve more accurate and detailed assessments of N distribution and uptake across different areas of their fields. This spatially resolved information supports targeted nutrient management strategies, reducing fertilizer use and improving crop yield. Furthermore, the flexibility and efficiency of UAVs in capturing real-time, high-resolution data make them a powerful tool for optimizing N fertilization practices and enhancing overall farm productivity. However, data processing may be time- and knowledge-intensive. High-altitude remote sensing using satellite imagery offers a large coverage area with less time-intensive data acquisition for end users. However, also in this case the data processing may require skilled labor or additional costs, and atmospheric and cloud conditions can affect data quality. Thus, satellite-based information products are often offered by specialized companies or governmental institutions. Cloud cover in some regions can affect in-season monitoring for optical satellites, such as Sentinel-2.

4.3.2. Digitization footprint

In terms of digitization footprints, based on the estimation done with the data of this study, the satellite platform appears to have the lower footprint while the two UAS platforms have the highest footprint. The digitation footprint concept (Marinello et al., 2019) was applied here by calculating the raw output information of the sensor as indicator. This is a relatively simple assessment, as it does not consider the necessary processing power needed to obtain final information that can be used by the farmers and neither the processing power of the tractor's computer, which may be comparable across devices with the exception of the tractor-mounted sensor. For that reason, it is not surprising that the UAS platforms, containing the highest level of spatial resolution among the investigated devices, show the highest footprint. In the future, such indicators should be actively used and be more standardized to assess also the impact of new technologies in terms of energy and resources required.

The digitization footprint varies significantly across sensor platforms due to differences in spectral and spatial resolution, affecting data volume, processing requirements, and practical usability. Hyperspectral sensors like ASD capture detailed spectral information (350–2500 nm) at a high data cost (~2.5 MB per spectrum), while multispectral UAV sensors (e.g., Micasense, Sequoia) balance data size (~1.6 GB per field) with agronomic relevance. Tractor-mounted ISARIA provides frequent, point-based measurements (~500 KB per field), optimizing real-time decision-making. Sentinel-2, though lower in resolution (10–30 m), offers scalable, cost-effective monitoring (~700 MB per scene). These differences influence sensor suitability for site-specific nitrogen management—high-resolution UAV and ground-based sensors enable precise within-field applications, while satellite imagery supports broader-scale assessments. Understanding this trade-off is critical for integrating data effectively in precision agriculture.

4.3.3. Economic aspect

In summary, the utilization of (pre-processed) satellite information theoretically presents an opportunity for the lowest costs per hectare and a reduced setup time, making this technology widely accessible to farmers and other users interested in spatial crop and field information. Extension services at the regional to national level could provide the information at a fixed cost per unit surface, as seen in large-scale business operations, reducing the time- and knowledge-investment which makes these technologies less attractive for farmers. Several missions, such as the Landsat and Copernicus missions from NASA and ESA, include a free data policy, thus widely increasing availability of high-quality data for different users. Alternatively, satellite-based information can be purchased from companies with prices ranging from 6 to 20 EUR/ha or annual subscriptions. Some examples are Earth Daily Agro and OneSoil at the global level, Farmstar-Conseil in France (Coquil and Bordes, 2005), VISTA in Germany other emerging start-ups globally. The adoption of optical sensors for N management in agriculture varies depending on factors such as farm size, technical knowledge, ease of integration, and data availability (Fabiani et al., 2020; Li et al., 2020; Lowenberg-DeBoer and Erickson, 2019). As technology becomes more accessible and affordable, the use of optical sensors is generally expected to increase (Groher et al., 2020). The environmental benefits of using these sensors, including reduced fertilizer inputs, coupled with specific subsidies may further promote their adoption (Späti et al., 2021).

4.3.4. Multi-source data integration

An additional aspect is the multi-source data integration of different sensors. In their review, Alvarez-Vanhard et al. (2021) report that data fusion is a powerful strategy in precision agriculture, combining multiple data sources to create enhanced datasets by integrating spatial, spectral, and temporal dimensions. Most studies focus on pixel-level fusion to improve time series data resolution, such as mapping intra-seasonal variations. More advanced methods include spatial-spectral fusion (e.g., using UAV imagery to improve satellite data resolution) and spatial–temporal fusion (e.g., combining UAV and satellite data to derive biophysical parameters). Some studies also explore feature-level fusion, such as integrating UAV and satellite data from different angles. For example, satellite data could be integrated by drone data, which offers higher spatial and temporal resolution for to address gaps in data caused by cloud cover and canopy closure (Zhou et al., 2025), providing a comprehensive and dynamic solution for precise operations at resolutions around 10×10 m pixels, such as section-controlled spraying and pneumatic fertilizer spreaders. Additionally, statistical modelling techniques, such as Bayesian Theory for Spectral Information Completion could be used to fill in missing spectral data in multispectral satellite images using hyperspectral UAV data, resulting in continuous spectral reflectance at high temporal frequency (Gevaert et al., 2015).

A final remark concerns the integration of other sources of information such as soil information and other environmental variables. In fact, optical sensors alone are often not sufficient to provide a full assessment of crop N status at field level. While soil and weather conditions undoubtedly influence crop growth and management decisions, their impact on the relationship between NDRE and nitrogen uptake is more nuanced. For instance, soil properties may affect this relationship in early growth stages due different optical properties in the background. However, weather conditions, when data collection follows best practices (e.g., no clouds, proper atmospheric and radiometric correction, and extensive model calibration), have a limited direct influence. Instead, crop- and cropping system-related factors, such as variety, seed density, and average leaf angle, play a more critical role in shaping NDRE responses. To address these issues, sensor information needs to be linked to soil information and environmental parameters through modeling or in-season data to understand if the crop is limited by nutrient availability (evaluation of soil mineral N) or by other factors such as drought (Argento et al., 2022; Crema et al., 2020; Kersebaum et al., 2005; Mittermayer et al., 2021; Zhang et al., 2020). In a recent study Guerrero et al. (2021) highlight the importance of data fusion for optimizing nitrogen fertilization in precision agriculture. By using combining soil data (e.g., pH, organic carbon, moisture content) collected through a high-resolution vis-NIR spectrophotometer with crop data such as NDVI and historical yield, the researchers created management zone maps to guide variable-rate nitrogen fertilization (VRNF). Integrating these aspects into precision agriculture strategies ensures a more robust interpretation of NDRE-based nitrogen assessments.

5. Conclusion and outlook

This case study shows that the five optical sensor platforms examined provide different information but appeared suitable for monitoring N status. However, selecting the appropriate sensor and platform depends on factors such as data availability, cost-efficiency, and ease of use. Users should consider the specific needs and limitations of each technology to make informed decisions for crop monitoring and nutrient management. Although all five sensor platforms can effectively monitor N status, they each have limitations. Satellite platforms are cost-effective and simple but face challenges with workflows and cloud cover, particularly for time-sensitive tasks. UASs offer high resolution and control but requires significant labor and expertise. Tractor-mounted sensors are automated and less labor-intensive but have moderate resolution and higher costs. Handheld platforms are best suited for small fields or research. The study found that resampling UAS-based maps to a 10-m resolution provided a good balance between spatial detail and machinery working width. The data used in this study were collected out of two sites in one year and therefore need replication to broaden the applicability of results for different pedo-climatic and seasonal conditions. However, other studies support these findings for winter wheat, suggesting that the use of these sensors across different climates, soils and seasons is reliable and not a significant concern. While the approach used in this study can be transferred to other crops, the results may not be directly comparable as different crops have unique growth characteristics, nutrient requirements, and responses to environmental conditions, which can influence the relationship between spectral indices and N uptake.

Sensor-based N status determination can enhance N use efficiency by addressing in-field variability of crop growth and supporting precision fertilization, provided there is accurate calibration for the specific climate and crop variety. At present, the use of all five optical sensor platforms is still increasing. Their values are well-correlated, indicating that they can all be used for monitoring N status. However, the significant variability in NDRE measurements across platforms underscores the importance of selecting the right device for effective nutrient management and calls for further research to investigate the sources of this variability to ensure more consistent and reliable data for N fertilization decision-making. The calibration of these sensors and the algorithms needed to determine optimal amounts of N fertilizer as well as the practical applicability on farms remain the main challenges for the future.

Declaration of Generative AI and AI-assisted technologies in the writing process.

During the preparation of this work the author(s) used ChatGPT 3.5 (OpenAI) and DeepL Write (DeepL) in order to check grammar and improve the language use of certain sections such as abstract, introduction, discussion and conclusion. After using this tool/service, the author(s) reviewed and edited the content as needed and take(s) full responsibility for the content of the publication. The text was additionally checked by an internal service of proof-reading within Agroscope (language experts, not AI-assisted).

CRediT authorship contribution statement

Francesco Argento: Writing – review & editing, Writing – original draft, Investigation, Formal analysis, Data curation, Conceptualization. **Quirina Merz:** Writing – review & editing, Investigation, Data curation. **Gregor Perich:** Writing – review & editing, Visualization, Investigation, Data curation. **Thomas Anken:** Writing – review & editing, Supervision, Resources, Project administration, Funding acquisition, Conceptualization. **Achim Walter:** Writing – review & editing, Supervision, Project administration, Funding acquisition, Conceptualization. **Frank Liebisch:** Writing – review & editing, Writing – original draft, Validation, Project administration, Conceptualization.

Declaration of competing interest

The authors declare the following financial interests/personal relationships which may be considered as potential competing interests: [Prof. Achim Walter reports financial support was provided by Federal Office for Agriculture and Agroscope. Dr. Thomas Anken reports financial support was provided by Agroscope. Prof. Achim Walter reports financial support was provided by Swiss National Science Foundation. Dr. Francesco Argento reports administrative support and equipment/ supplies were provided by ETH Zurich and Agroscope. All the optical sensor platforms used for the study were commercially available during the time of the study and were available at the institutions of the authors, except for the tractor-mounted sensor Isaria from the german company Fritzmeier which was provided and used by the project partner and land manager Swiss Future Farm. There was no economic or personal interest to promote the use of a particular technology in the study. If there are other authors, they declare that they have no known competing financial interests or personal relationships that could have appeared to influence the work reported in this paper].

Acknowledgements

The authors would like to thank those who contributed conceptually or technically to the realization of the study. We would like to thank Michael Simmler (Agroscope) and Helge Aasen (Agroscope) for their conceptual and practical contributions to the study and the paper. We are grateful to Matthias Hatt (Agroscope), Eric Vogelsanger (Agroscope), and Brigitta Herzog (ETH Zurich) for their help with the field experiment and sample processing. Moreover, we would like to thank the Swiss Future Farm, especially Florian Abt, for the technical support in the management of the field experiments and data collection. The main project that supported this study, DigiN, was funded by Agroscope through a special fund supervised by the Swiss Federal Office for Agriculture (FOAG). The sampling campaign, as well as part of the data analysis, was also carried out in the framework of two other projects at ETH Zürich: DeepField, funded by the FOAG and InnoFarm, funded by the Swiss National Science Foundation (SNSF) in the framework of the national research program 73 (grant nr. 407340_172433).

Data availability

The dataset associated with this study is available in the Mendeley Data Repository at the following link: DOI: 10.17632/639wzh2n8f.1

References

Adamchuk, V.I., Hummel, J.W., Morgan, M.T., Upadhyaya, S.K., 2004. On-the-go soil sensors for precision agriculture. Comput. Electron. Agric. 44, 71–91. https://doi.org/10.1016/j.compag.2004.03.002.

Alvarez-Vanhard, E., Corpetti, T., Houet, T., 2021. UAV & satellite synergies for optical remote sensing applications: a literature review. *Sci. Remote Sens.* 3, 100019. https://doi.org/10.1016/j.srs.2021.100019.

Argento, F., 2021. Combined digital and standard methods to optimize nitrogen (N) management and reduce N surplus in winter wheat (T aestivum) production (Doctoral Thesis). ETH Zurich. https://doi.org/10.3929/ethz-b-000493036.

Argento, F., Anken, T., Abt, F., Vogelsanger, E., Walter, A., Liebisch, F., 2020. Site-specific nitrogen management in winter wheat supported by low-altitude remote sensing and soil data. Precis. Agric. https://doi.org/10.1007/s11119-020-09733-3.

Argento, F., Liebisch, F., Simmler, M., Ringger, C., Hatt, M., Walter, A., Anken, T., 2022. Linking soil N dynamics and plant N uptake by means of sensor support. Eur. J. Agron. 134, 126462. https://doi.org/10.1016/j.eja.2022.126462.

Aula, L., Omara, P., Nambi, E., Oyebiyi, F.B., Raun, W.R., 2020. Review of active optical sensors for improving winter wheat nitrogen use efficiency. Agronomy 10 (8), 1157.

Barnes, E. M., Clarke, T. R., Richards, S. E., Colaizzi, P. D., Haberland, J., Kostrzewski, M.,… and Moran, M. S., 2000. Coincident detection of crop water stress, nitrogen status and canopy density using ground based multispectral data. In *Proceedings of the fifth international conference on precision agriculture, Bloomington, MN, USA* (Vol. 1619, No. 6).

Basso, B., Fiorentino, C., Cammarano, D., Schulthess, U., 2016. Variable rate nitrogen fertilizer response in wheat using remote sensing. Precis. Agric. 17, 168–182. https://doi.org/10.1007/s11119-015-9414-9.

Bean, G.M., Kitchen, N.R., Camberato, J.J., Ferguson, R.B., Fernandez, F.G., Franzen, D. W., Laboski, C.A.M., Nafziger, E.D., Sawyer, J.E., Scharf, P.C., Schepers, J., Shanahan, J.S., 2018. Active-optical reflectance sensing corn algorithms evaluated over the United States Midwest corn belt. Agron. J. 110, 2552–2565. https://doi.org/10.2134/agronj2018.03.0217.

Bendig, J., Yu, K., Aasen, H., Bolten, A., Bennertz, S., Broscheit, J., Gnyp, M.L., Bareth, G., 2015. Combining UAV-based plant height from crop surface models, visible, and near infrared vegetation indices for biomass monitoring in barley. Int. J. Appl. Earth Obs. Geoinformation 39, 79–87. https://doi.org/10.1016/j.jag.2015.02.012.

Berger, K., Verrelst, J., Féret, J.B., Wang, Z., Wocher, M., Strathmann, M., Danner, M., Mauser, W., Hank, T., 2020. Crop nitrogen monitoring: Recent progress and principal developments in the context of imaging spectroscopy missions. Remote Sens. Environ. 242, 111758. https://doi.org/10.1016/j.rse.2020.111758.

Cammarano, D., Fitzgerald, G., Basso, B., O'Leary, G., Chen, D., Grace, P., Fiorentino, C., 2011. Use of the Canopy Chlorophyl Content Index (CCCI) for remote estimation of wheat nitrogen content in rainfed environments. Agron. J. 103, 1597–1603. https://doi.org/10.2134/agronj2011.0124.

Chunjiang, Z., Aning, J., Wenjiang, H., Keli, L., Liangyun, L., Jihua, W., 2007. Evaluation of variable-rate nitrogen recommendation of winter wheat based on SPAD chlorophyll meter measurement. N. z. J. Agric. Res. 50, 735–741. https://doi.org/10.1080/00288230709510345.

Clay, D.E., Kharel, T.P., Reese, C., Beck, D., Carlson, C.G., Clay, S.A., Reicks, G., 2012. Winter wheat crop reflectance and nitrogen sufficiency index values are influenced by nitrogen and water stress. Agron. J. 104, 1612–1617. https://doi.org/10.2134/agronj2012.0216.

Cohan, J., Soenen, B., Vericel, G., Laurent, F., 2018. Improving nitrogen use efficiency in wheat: recent progress and prospects in France. Proceedings of Phloème, first biennials of cereal innovation, Paris, 24th–25th January.

Colaço, A.F., Bramley, R.G., 2018. Do crop sensors promote improved nitrogen management in grain crops? Field Crop Res 218, 126–140.

Coquil, B., Bordes, J.P., 2005. FARMSTAR: An efficient decision support tool for near real time crop management from satellite images. Precis. Agric.

Corti, M., Cavalli, D., Cabassi, G., Marino Gallina, P., Bechini, L., 2018. Does remote and proximal optical sensing successfully estimate maize variables? A review. Eur. J. Agron. 99, 37–50. https://doi.org/10.1016/j.eja.2018.06.008.

Crema, A., Boschetti, M., Nutini, F., Cillis, D., Casa, R., 2020. Influence of soil properties on maize and wheat nitrogen status assessment from Sentinel-2 data. Remote Sens. 12. https://doi.org/10.3390/rs12142175.

Diacono, M., Rubino, P., Montemurro, F., 2013. Precision nitrogen management of wheat. A Review. Agron. Sustain. Dev. 33, 219–241. https://doi.org/10.1007/s13593-012-0111-z.

ESA, 2023. European space agency, Copernicus Sentinel-2 collection. Collection 1 Level-2A - Sentinel Online (copernicus.eu) [last accessed on 12.09.2024].

Fabiani, S., Vanino, S., Napoli, R., Zajíček, A., Duffková, R., Evangelou, E., Nino, P., 2020. Assessment of the economic and environmental sustainability of variable rate technology (VRT) application in different wheat intensive European agricultural areas. a Water energy food nexus approach. Environ. Sci. Policy 114, 366–376. https://doi.org/10.1016/j.envsci.2020.08.019.

Féret, J.-B., 2011. Optimizing spectral indices and chemometric analysis of leaf chemical properties using radiative transfer modeling. Remote Sens Environ.

Franzen, D., Kitchen, N., Holland, K., Schepers, J., Raun, W., 2016. Algorithms for in-season nutrient management in cereals. Agron. J. https://doi.org/10.2134/agronj2016.01.0041.

Gabriel, J.L., Zarco-Tejada, P.J., López-Herrera, P.J., Pérez-Martín, E., Alonso-Ayuso, M., Quemada, M., 2017. Airborne and ground level sensors for monitoring nitrogen status in a maize crop. Biosyst. Eng. 160, 124–133. https://doi.org/10.1016/j.biosystemseng.2017.06.003.

Gevaert, C.M., Suomalainen, J., Tang, J., Kooistra, L., 2015. Generation of spectral–temporal response surfaces by combining multispectral satellite and hyperspectral UAV imagery for precision agriculture applications. *IEEE J. Sel. Top. Appl. Earth Obs. Remote Sens.* 8 (6), 3140–3146.

Gillies, S. et al., 2013. Rasterio: geospatial raster i/o for Python programmers. https://github.com/rasterio/rasterio [last accessed on 12.09.2024].

Gnyp, M., Panitzki, M., Reusch, S., Bareth, G., 2016. Comparison between tractor-based and UAV-based spectrometer measurements in winter wheat. 13th Int. Conf. Precis. Agric, 1–10.

Graf, L.V., Perich, G., Aasen, H., 2022. EOdal: An open-source Python package for large-scale agroecological research using Earth Observation and gridded environmental data. Comput. Electron. Agric. 203, 107487. https://doi.org/10.1016/j.compag.2022.107487.

Groher, T., Heitkämper, K., Walter, A., Liebisch, F., Umstätter, C., 2020. Status quo of adoption of precision agriculture enabling technologies in Swiss plant production. Precis. Agric. 21, 1327–1350. https://doi.org/10.1007/s11119-020-09723-5.

Guerrero, A., De Neve, S., Mouazen, A.M., 2021. Data fusion approach for map-based variable-rate nitrogen fertilization in barley and wheat. *Soil Tillage Res.* 205, 104789. https://doi.org/10.1016/j.still.2020.104789.

Guyot, G., Baret, F., Major, D.J., 1988. High spectral resolution: determination of spectral shifts between the red and infrared. Int. Arch. Photogramm. Remote Sens. 11, 750–760. https://doi.org/10.1093/mind/VII.25.101.

Heege, H.J., Reusch, S., Thiessen, E., 2008. Prospects and results for optical systems for site-specific on-the-go control of nitrogen-top-dressing in Germany. Precis. Agric. 9, 115–131. https://doi.org/10.1007/s11119-008-9055-3.

Holland, K.H., Schepers, J.S., 2010. Derivation of a variable rate nitrogen application model for in-season fertilization of corn. Agron. J. 102, 1415–1424. https://doi.org/10.2134/agronj2010.0015.

Isaac, W., Na, A., 2016. On-the-go soil nitrogen sensor based on near infrared spectroscopy. Presented at the 2016 International Conference on Information Technology (InCITe) - The Next Generation IT Summit on the Theme - Internet of Things: Connect your Worlds, pp. 312–315. Doi: 10.1109/INCITE.2016.7857637.

Jiang, J., Wang, C., Wang, H., Fu, Z., Cao, Q., Tian, Y., Zhu, Y., Cao, W., Liu, X., 2021. Evaluation of three portable optical sensors for non-destructive diagnosis of nitrogen status in winter wheat. Sensors 21, 5579. https://doi.org/10.3390/s21165579.

Jin, Z., Prasad, R., Shriver, J., Zhuang, Q., 2017. Crop model- and satellite imagery-based recommendation tool for variable rate N fertilizer application for the US corn system. Precis. Agric. 18. https://doi.org/10.1007/s11119-016-9488-z.

Jordan-Meille, L., Denoroy, P., Dittert, K., Cugnon, T., Quemada, M., Wall, D., Bechini, L., Marx, S., Oenema, O., Reijneveld, A., Liebisch, F., Diedhiou, K., Degan, F., Higgins, S., 2023. Comparison of nitrogen fertilisation recommendations of West European Countries. Eur. J. Soil Sci. 74, e13436. https://doi.org/10.1111/ejss.13436.

Kersebaum, K.C., Lorenz, K., Reuter, H.I., Schwarz, J., Wegehenkel, M., Wendroth, O., 2005. Operational use of agro-meteorological data and GIS to derive site specific nitrogen fertilizer recommendations based on the simulation of soil and crop growth processes. Phys. Chem. Earth 30, 59–67. https://doi.org/10.1016/j.pce.2004.08.021.

Kindred, D.R., Milne, A.E., Webster, R., Marchant, B.P., Sylvester-Bradley, R., 2015. Exploring the spatial variation in the fertilizer-nitrogen requirement of wheat within fields. J. Agric. Sci. 153, 25–41. https://doi.org/10.1017/S0021859613000919.

Koch, B., Khosla, R., Frasier, W.M., Westfall, D.G., Inman, D., 2004. Economic feasibility of variable-rate nitrogen application utilizing site-specific management zones. Agron. J. 96, 1572–1580. https://doi.org/10.2134/agronj2004.1572.

Li, D., Zhang, P., Chen, T., Qin, W., 2020. Recent development and challenges in spectroscopy and machine vision technologies for crop nitrogen diagnosis: a review. Remote Sens. 12, 2578. https://doi.org/10.3390/rs12162578.

Li, F., Miao, Y., Feng, G., Yuan, F., Yue, S., Gao, X., Liu, Y., Liu, B., Ustin, S.L., Chen, X., 2014. Improving estimation of summer maize nitrogen status with red edge-based spectral vegetation indices. Field Crops Res. 157, 111–123. https://doi.org/10.1016/j.fcr.2013.12.018.

Li, J., Shi, Y., Veeranampalayam-Sivakumar, A.-N., Schachtman, D.P., 2018. Elucidating sorghum biomass, nitrogen and chlorophyll contents with spectral and morphological traits derived from unmanned aircraft system. Front. Plant Sci. 9, 1–12. https://doi.org/10.3389/fpls.2018.01406.

Liebisch, F., Küng, G., Damm, A., Walter, A., 2014. Characterization of crop vitality and resource use efficiency by means of combining imaging spectroscopy based plant traits. Workshop Hyperspectral Image Signal Process. Evol. Remote Sens. 2014-June. Doi: 10.1109/WHISPERS.2014.8077612.

Lowenberg-DeBoer, J., Erickson, B., 2019. Setting the record straight on precision agriculture adoption. Agron. J. 111, 1552–1569. https://doi.org/10.2134/agronj2018.12.0779.

Magney, T.S., Eitel, J.U.H., Vierling, L.A., 2017. Mapping wheat nitrogen uptake from RapidEye vegetation indices. Precis. Agric. 18. https://doi.org/10.1007/s11119-016-9463-8.

Manuilova, E. Schuetzenmeister A., 2021. "mcr": Method comparison regression. R package version 1.2.2. https://CRAN.R-project.org/package=mcr.

Meier, U., Bleiholder, H., Buhr, L., Feller, C., Hack, H., Heß, M., et al., 2009. The BBCH system to coding the phenological growth stages of plants–history and publications. "Journal Für Kulturpflanzen" 61 (2), 41–52.

Merz, Q. N., 2022. From Leaf to Landscape Spatio-temporal monitoring of crops to improve decision support (Doctoral dissertation, ETH Zurich). Doi: 10.3929/ethz-b-000602455.

Marinello, F., Bramley, R.G.V., Cohen, Y., Fountas, S., Guo, H., Karkee, M., Martínez-Casasnovas, J.A., Paraforos, D.S., Sartori, L., Sorensen, C.G., Stenberg, B., Sudduth, K., Tisseyre, B., Vellidis, F., Vougioukas, S.G., 2019. Agriculture and digital sustainability: a Digitization Footprint, in: Precision Agriculture '19. Wageningen Academic, pp. 83–89. Doi: 10.3920/978-90-8686-888-9_9.

Mittermayer, M., Gilg, A., Xaver, F., Ludwig, M., 2021. Site - specific nitrogen balances based on spatially variable soil and plant properties. Precis. Agric. https://doi.org/10.1007/s11119-021-09789-9.

Mulla, D.J., 2013. Twenty-five years of remote sensing in precision agriculture: key advances and remaining knowledge gaps. Biosyst. Eng. 114 (4), 358–371.

Muñoz-Huerta, R.F., Guevara-Gonzalez, R.G., Contreras-Medina, L.M., Torres-Pacheco, I., Prado-Olivarez, J., Ocampo-Velazquez, R.V., 2013. A review of methods for sensing the nitrogen status in plants: advantages, disadvantages and recent advances. Sens. Switz. 13, 10823–10843. https://doi.org/10.3390/s130810823.

Padilla, F.M., Gallardo, M., Peña-Fleitas, M.T., De Souza, R., Thompson, R.B., 2018. Proximal optical sensors for nitrogen management of vegetable crops: a review. Sensors 18, 2083. https://doi.org/10.3390/s18072083.

Perich, G., Aasen, H., Verrelst, J., Argento, F., Walter, A., Liebisch, F., 2021. Crop nitrogen retrieval methods for simulated sentinel-2 data using in-field spectrometer data. Remote Sens. (Basel) 13 (12), 2404. https://doi.org/10.3390/rs13122404.

Perich, G., Turkoglu, M.O., Graf, L.V., Wegner, J.D., Aasen, H., Walter, A., Liebisch, F., 2023. Pixel-based yield mapping and prediction from Sentinel-2 using spectral indices and neural networks. Field Crop Res 292, 108824. https://doi.org/10.1016/j.fcr.2023.108824.

Prey, L., Schmidhalter, U., 2019. Sensitivity of vegetation indices for estimating vegetative N status in winter wheat. Sensors 19 (17), 3712.

QGIS Development Team, 2023. QGIS geographic information system. Open-source geospatial foundation project. Retrieved June 9, 2020, from http://qgis.osgeo.org [last accessed on 12.09.2024].

R Core Team, 2024. R: A language and environment for statistical computing. R Foundation for Statistical Computing: Vienna, Austria.

Raj, R., Kar, S., Nandan, R., Jagarlapudi, A., 2020. Precision agriculture and unmanned aerial Vehicles (UAVs). Unmanned aerial vehicle: Applications in agriculture and environment, 7-23.

Raun, W.R., Solie, J.B., Stone, M.L., Martin, K.L., Freeman, K.W., Mullen, R.W., Zhang, H., Schepers, J.S., Johnson, G.V., 2005. Optical sensor-based algorithm for crop nitrogen fertilization. Commun. Soil Sci. Plant Anal. 36, 2759–2781. https://doi.org/10.1080/00103620500303988.

Roberts, D.F., Ferguson, R.B., Kitchen, N.R., Adamchuk, V.I., Shanahan, J.F., 2012. Relationships between soil-based management zones and canopy sensing for corn Nitrogen management. Agron. J. 104, 119–129. https://doi.org/10.2134/agronj2011.0044.

Samborski, S.M., Tremblay, N., Fallon, E., 2009. Strategies to make use of plant sensors-based diagnostic information for nitrogen recommendations. Agron. J. 101, 800–816. https://doi.org/10.2134/agronj2008.0162Rx.

Scharf, P.C., Schmidt, J.P., Kitchen, N.R., Sudduth, K.A., Hong, S.Y., Lory, J.A., Davis, J. G., 2002. Remote sensing for nitrogen management. J. Soil Water Conserv. 57, 518–524.

Sharma, L.K., Bali, S.K., 2017. A review of methods to improve nitrogen use efficiency in agriculture. Sustainability 10 (1), 51.

Sinaj, S., Richner, W., 2017. Principles of fertilization of agricultural crops in Switzerland (PRIF 2017). Agrarforsch. Schweiz 8 (6).

Signorell, A., 2021. "DescTools": Tools for Descriptive Statistics. R package version 0.99.42. https://cran.r-project.org/package=DescTools.

Singh, M., Kumar, R., Sharma, A., Singh, B., Thind, S.K., 2015. Calibration and algorithm development for estimation of nitrogen in wheat crop using tractor mounted N-sensor. Sci. World J. 2015. https://doi.org/10.1155/2015/163968.

Späti, K., Huber, R., Finger, R., 2021. Benefits of increasing information accuracy in variable rate technologies. Ecol. Econ. 185, 107047. https://doi.org/10.1016/j.ecolecon.2021.107047.

Stamatiadis, S., Schepers, J.S., Evangelou, E., Tsadilas, C., Glampedakis, A., Glampedakis, M., Dercas, N., Spyropoulos, N., Dalezios, N.R., Eskridge, K., 2018. Variable-rate nitrogen fertilization of winter wheat under high spatial resolution. Precis. Agric. 19, 570–587. https://doi.org/10.1007/s11119-017-9540-7.

Tremblay, N., Fallon, E., Ziadi, N., 2011. Sensing of crop nitrogen status: opportunities. Tools, Limitations, and Supporting Information Requirements. https://doi.org/10.21273/HORTTECH.21.3.274.

Tucker, C.J., 1979. Red and photographic infrared linear combinations for monitoring vegetation. Remote Sens. Environ. 8 (2), 127–150.

Verling, S., Stastny, T., Bättig, G., Alexis, K., Siegwart, R., 2017. Model-based transition optimization for a VTOL tailsitter. In: 2017 IEEE International Conference on Robotics and Automation (ICRA). IEEE, pp. 3939–3944.

Walter, A., Finger, R., Huber, R., Buchmann, N., 2017. Smart farming is key to developing sustainable agriculture. Proc. Natl. Acad. Sci. 114 (24), 6148–6150.

Wang, H., He, Z., Wang, S., Zhang, Y., Tang, H., 2024. Radiometric cross-calibration of GF6-PMS and WFV sensors with sentinel 2-MSI and landsat 9-OLI2. Remote Sens. 16, 1949. https://doi.org/10.3390/rs16111949.

Wang, K., Huggins, D.R., Tao, H., 2019. Rapid mapping of winter wheat yield, protein, and nitrogen uptake using remote and proximal sensing. Int. J. Appl. Earth Obs. Geoinformation 82, 101921. https://doi.org/10.1016/j.jag.2019.101921.

Warner, T.A., Nellis, M.D., Foody, G.M., 2009. Remote sensing scale and data selection issues. In: Foody, G.W.T., Nellis, M.D. (Eds.), The Sage Handbook of Remote Sensing. Sage, New York, pp. 1–17.

Williams, A., Davis, A.S., Ewing, P.M., Grandy, A.S., Kane, D.A., Koide, R.T., Mortensen, D.A., Smith, R.G., Snapp, S.S., Spokas, K.A., Yannarell, A.C., Jordan, N. R., 2016. Precision control of soil nitrogen cycling via soil functional zone management. Agric. Ecosyst. Environ. 231. https://doi.org/10.1016/j.agee.2016.07.010.

Yao, X., Huang, Y., Shang, G., Zhou, C., Cheng, T., Tian, Y., Cao, W., Zhu, Y., 2015. Evaluation of six algorithms to monitor wheat leaf nitrogen concentration. Remote Sens. 7, 14939–14966. https://doi.org/10.3390/rs71114939.

Zhang, J., Chen, Y., Zhang, Z., 2020. A remote sensing-based scheme to improve regional crop model calibration at sub-model component level. Agric. Syst. 181, 102814. https://doi.org/10.1016/j.agsy.2020.102814.

Zhao, B., Duan, A., Ata-Ul-Karim, S.T., Liu, Z., Chen, Z., Gong, Z., Zhang, J., Xiao, J., Liu, Z., Qin, A., Ning, D., 2018. Exploring new spectral bands and vegetation indices for estimating nitrogen nutrition index of summer maize. Eur. J. Agron. 93. https://doi.org/10.1016/j.eja.2017.12.006.

Zhou, Y., Ma, Y., Ata-Ul-Karim, S.T., Wang, S., Ciampitti, I., Antoniuk, V., Wu, C., Neumann Andersen, M., Cammarano, D., 2025. Integrating multi-angle and multi-scale remote sensing for precision nitrogen management in agriculture: a review. Comput. Electron. Agric. 230, 109829. https://doi.org/10.1016/j.compag.2024.109829.